Vertical seismic profile (VSP) in the JAPEX/JNOC/GSC Mallik 2L-38 gas hydrate research well

R. Walia[1], Y. Mi[2], R.D. Hyndman[3], and A. Sakai[4]

Walia, R., Mi, Y., Hyndman, R.D., and Sakai, A., 1999: Vertical seismic profile (VSP) in the JAPEX/JNOC/GSC Mallik 2L-38 gas hydrate research well; in *Scientific Results from JAPEX/JNOC/GSC Mallik 2L-38 Gas Hydrate Research Well, Mackenzie Delta, Northwest Territories, Canada, (ed.) S.R. Dallimore, T. Uchida, and T.S. Collett; Geological Survey of Canada, Bulletin 544, p. 341–355.*

Abstract: As part of the JAPEX/JNOC/GSC Mallik 2L-38 field program, a vertical seismic profiling(VSP) survey was carried out at zero and offset-source positions with multicomponent receiver tools and multipolarized vibrators. The results will be integrated with downhole logs and regional seismic data to evaluate the effect of gas hydrate on seismic velocity and to estimate gas hydrate concentrations. The excellent data quality allows accurate compressional-and shear-velocity depth profiles. There are down-going and up-going waves from numerous reflectors, and corridor stacks provide comparison with surface multichannel data. Velocities in the permafrost zone above 600 m are enhanced, to more than 2500 m/s. In the largely unfrozen section from 600 m to 850 m, the velocities are lower, about 2000 m/s. The gas hydrate zone is well defined below about 900 m, with velocities of 2500–2700 m/s. Poisson's Ratio is ~0.39 in both the permafrost and gas hydrate sections, compared to ~0.44 in the unfrozen sections.

Résumé : Un profilage sismique vertical a été effectué à la position zéro et aux positions déportées de la source à l'aide d'enregistreurs multicomposants et de vibrateurs multipolarisés dans le cadre de la campagne de terrain du projet JAPEX/JNOC/GSC Mallik 2L-38. Les résultats seront intégrés aux diagraphies en sondage et aux données sismiques régionales afin d'évaluer l'incidence des hydrates de gaz sur la vitesse des ondes sismiques et de faire l'estimation des concentrations des hydrates de gaz. Les excellentes données permettent d'établir avec précision des profils de célérité pour les ondes de compression et les ondes de cisaillement en fonction de la profondeur. De nombreux réflecteurs réfléchissent des ondes descendantes et ascendantes; la sommation sismique le long d'un couloir centré sur les premières arrivées devrait permettre d'établir une comparaison avec les données de sismique multicanal de surface. Les vitesses enregistrées dans la zone de pergélisol au-dessus de 600 m augmentent au-delà de 2 500 m/s. Dans la section en grande partie non gelée située entre 600 et 850 m, elles sont moins élevées, soit de l'ordre de 2 000 m/s. La zone des hydrates de gaz est bien définie au-dessous de 900 m environ et les vitesses s'échelonnent de 2 500 à 2 700 m/s. Le coefficient de Poisson est d'environ 0,39 dans la section à pergélisol et dans la section à hydrates de gaz et d'environ 0,44 dans les sections non gelées.

[1] CGG Geophysics Canada, Suite 700, 404 6th Avenue S.W., Calgary, Alberta, Canada T2P 0R9
[2] CREWES Project, Geology and Geophysics Department, University of Calgary, Calgary, Alberta, Canada T2N 1N4
[3] Geological Survey of Canada, Pacific Geoscience Centre, 8860 West Saanich Road, P.O. Box 6000, Sidney, British Columbia, Canada V8L 4B2
[4] Japan Petroleum Exploration Company, Ltd. (JAPEX), 2-2-20 Higashi-shinagawa, Shinagawa-ku, Tokyo 140-0002, Japan

INTRODUCTION

The JAPEX/JNOC/GSC Mallik 2L-38 gas hydrate research well was drilled in the Canadian Arctic to investigate gas hydrate in a permafrost setting, in a collaborative research project between the Japan National Oil Corporation (JNOC), and the Geological Survey of Canada (GSC). Other principal participants in the project included Japan Petroleum Exploration Company Limited (JAPEX), and the United States Geological Survey (USGS), along with a number of other Japanese and North American institutes and companies. The 1150 m deep well is located in the Mackenzie Delta, Northwest Territories, Canada, at lat. 69°27′40.71″N, and long. 134°39′30.37″W, elevation 1.1 m. The datum reference (kelly bushing) is 8.31 m above mean sea level (Fig. 1). The well was part of a Japanese government-industry program to assess the potential of gas hydrate as an energy source. The project was intended to evaluate drilling, coring, and geophysical technologies prior to an offshore gas hydrate research well planned for off southwest Japan by JNOC in 1999. The overall objectives, program management, and operations were described by Dallimore et al. (1999) and Dallimore (http://sts.gsc.nrcan.gc.ca/page1/hydrat/fact_i.html, 1998). The multidisciplinary study included permafrost and gas hydrate coring, comprehensive downhole geophysical logging and measurement, and a deep sounding electromagnetic survey. A high-resolution multichannel seismic survey is planned. Laboratory studies on recovered cuttings and core included sedimentology, physical properties, geochemistry, and reservoir characteristics of the Mallik 2L-38 gas accumulation.

As part of the Mallik 2L-38 field program, a vertical seismic profiling survey (VSP) was carried out at zero and offset-source positions with multicomponent receiver tools and multipolarized vibrator sources. The survey was carried out with by Schlumberger Ltd. in March 1998, with field-operation planning and direction by A. Sakai of JAPEX (Sakai, 1998, 1999). A special effort was made to record high-quality shear-wave data as well as compressional-wave data. Results from this work will be integrated with downhole logs and regional seismic data. The data will also be used to determine the effect of gas hydrate on formation velocities and to estimate gas hydrate concentrations as a function of depth in the formation penetrated by the well. Two research teams were involved in the analysis of the VSP data, one in Japan (Sakai, 1998, 1999) and one in Canada. This report gives a description of the processing and initial results from the Canadian team. The analysis used the ITA-Insight processing package. Hardage (1983) and Toksoz and Stewart (1983) discussed some of the processing principles.

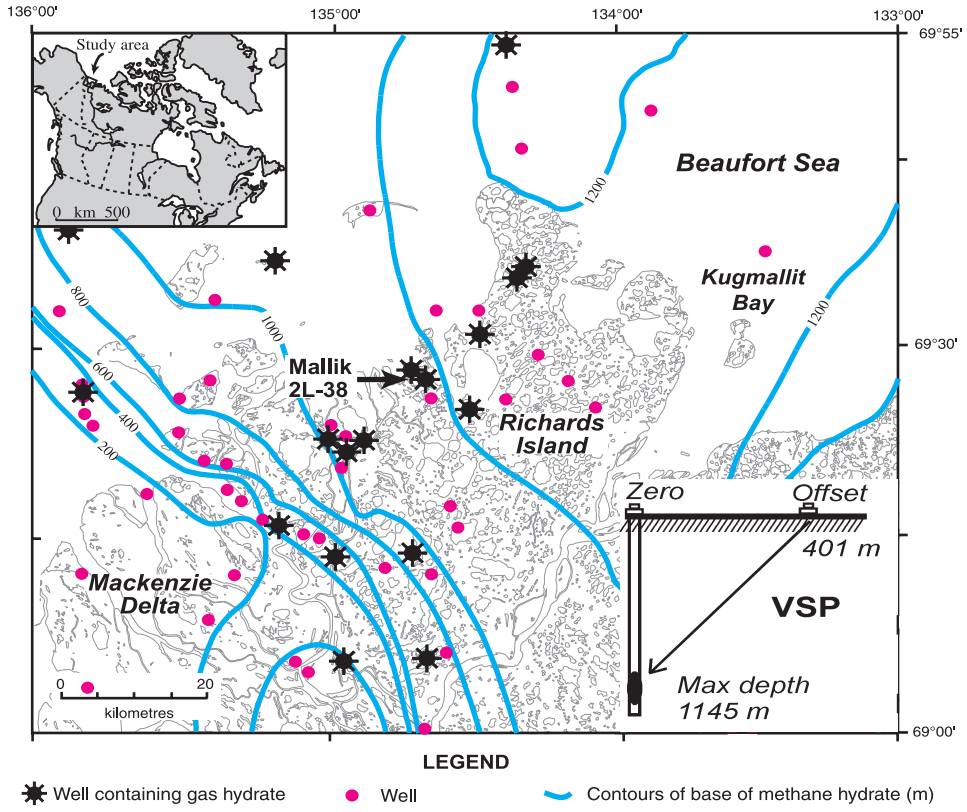

Figure 1. *Location map of the Mackenzie Delta region in the Canadian Arctic showing the location of the Mallik 2L-38 well. The inset shows the geometry of the VSP vertical and offset recording for the Mallik well.*

Table 1. Files dedicated to different components.

File	Offset	Component	Receiver depth interval (m)	Depth range
1–11	Zero	X(Vertical and horizontal vibration)	5 m for vertical vibration 15 m for horizontal vibration	500 m to 1145 m
12–22		Y(Vertical and horizontal vibration)		
23–33		Z(Vertical and horizontal vibration)		
34–41	400.7 m	X(Vertical vibration only)	5 m for vertical vibration	240 m to 1145 m
42–49		Y (Vertical vibration only)		
50–57		Z(Vertical vibration only)		

VSP SURVEY AND DATA

Sakai (1998, 1999) described the VSP survey parameters. The two sources were IVI MiniVibrators for compressional and shear modes (transverse to the well). The zero-offset recording was from 500 to 1145 m depth at intervals of 5 m for the compressional source, and 15 m for the shear source in transverse mode. For the offset VSP, recording was from 240 to 1145 m, and the compressional source was recorded at 5 m intervals. The source was a 12 s linear sweep with frequency band 10–200 Hz for the zero-offset compressional source, 10–100 Hz for the offset compressional source, and 10–50 Hz for the zero-offset shear source. The low pass allowed more energy in the frequency band found to have the least noise. The listen time was 3 s and the sampling rate was 1 ms. The zero-offset source was 40 m from the well head. The offset source was 401 m from the well, approximately on the line of a previous surface seismic survey. This was found to be the maximum distance for a good signal. Sakai (1998, 1999) described the special efforts to optimize the coupling of the vibrator to the ground and to reduce ambient noise in the permafrost environment. Wind noise was an important problem affecting the data quality, especially for the lower frequency shear-wave data.

Downhole recording employed two directly connected Schlumberger three-component Combined Seismic Imager (CSI) tools, with a 300 Hz low-pass filter. The hole was cased above 676 m; in the upper 250 m the casing contact with the formation was poor and the recorded signals were weak. In the open-hole portion, the previously collected downhole logs were used to select the optimal receiver positions and to avoid caved zones. Vertical- and horizontal-vibration data were recorded alternately. There were nominally five recorded traces for each receiver depth, but more vibrator shots were carried out if the data quality was poor. There were several test shots at irregular receiver depths; they were included in the data reorganization and sorting, but excluded in further processing, especially in wavefield separation.

The VSP data initially processed in this study are listed in Table 1.

DATA PROCESSING

The processing completed so far in this study was mainly for the zero-offset vertical-vibration Z-component data and offset vertical-vibration Z-component data. Zero-offset horizontal-vibration X-component data has also been processed in an effort to recover shear-wave sections, but there were hardly any events that could be seen in this component. Preliminary processing has been done on other zero-offset and offset data; however, it has been very difficult to separate the P- and S-wavefields without distortion. First arrivals were picked for the zero-offset vertical-vibration Z-component data (P-wave), horizontal-vibration X-component data (S-wave), and offset Z-component data (P-wave). Interval P- and S-wave velocities were calculated. For higher resolution in first-arrival picking, the vertical-vibration Z-component data were resampled to 125 μs from the recorded 1 ms sample rate. The horizontal-vibration X-component data were resampled to 250 μs sample rate.

Extensive trace editing was done before processing. First arrivals in traces with high noise or irregular depths were removed. An advantage of VSP data processing is that the embedded wavelet can be estimated from the down-going wavefield and an inverse filter can be derived and applied to the up-going wavefield. We applied deterministic wavelet deconvolution on the zero-offset and offset-source vertical-vibration Z-component data. However, strong harmonic noise prevented us from estimating a reliable wavelet so that zero-phase spiking deconvolution was also tested. The result of spiking deconvolution appears clearer. The wavelet-processing flow is shown in Table 2: a) wavelet-processing flow and b) spiking-deconvolution flow. For phase interpretation, we also generated a Rieber mixing section by passing the horizontal events in the F-K (frequency-wavenumber) domain for the aligned up-going wavefield after application of spiking deconvolution.

The horizontal-vibration X-component data had both 5 m and 15 m depth-receiver intervals, and the survey geometry was not uniform between the shallower part (<675 m) and the deeper part (>675 m) of the well. Dummy traces were therefore inserted to form a regular depth interval of 5 m. However, wavefield separation in F-K domain was not successful because of the number of dummy traces. The shear-wave velocity profile derived from the first arrivals is the main result from this component.

Table 2a. Wavelet-processing flow.

Processing steps	Description
1	Data extraction.
2	Format conversion SEG-Y -> ITA
3	Source type and component separation
4	Trace editing
5	Geometrical spreading correction: time power 1.0
6	3-loop trim statics application
7	Ensemble amplitude balancing
8	Stacking at constant recording depth, resampling, and first arrival picking.
9	F-X noise reduction.
10	F-K domain wavefield separation.
11	Wavelet extraction, inverse-filter calculation and application on up-going wavefield.
12	Corridor stack of up-going wavefield.

Table 2b. Zero-phase spiking-deconvolution flow.

Processing steps	Description
1	Data extraction.
2	Format conversion SEG-Y -> ITA
3	Source type and component separation
4	Trace editing
5	Geometrical spreading correction: time power 1.0
6	Zero-phase spiking-deconvolution operator length:120 ms, band pass filter 10-20-25-140
7	3-loop trim statics application
8	Ensemble amplitude balancing
9	Stacking at constant recording depth and first arrival picking
10	F-X noise reduction.
11	F-K domain wavefield separation.
12	Reiber mixing of up-going wavefield, corridor stack of up-going wavefield.

ANALYSIS RESULTS

Wavefield plots

Figure 2 shows a series of plots representing progressive processing steps. The left column of displays is from zero-phase, spiking-deconvolution processing flow while the right column of displays is from wavelet-processing flow. Figure 2 shows a) the raw data after sorting and initial editing, only the first trace in each common-depth-receiver gather is shown; b) processed full wavefield, the section for following wavelet processing does not have zero-phase spiking deconvolution applied; c) down-going wavefield; d) up-going wavefield; e) aligned up-going wavefield; f) corridor selected for corridor stack and (at right) the stacking result in positive and negative polarity; g) aligned up-going wavefield after Rieber mixing; and h) wavelet extracted from down-going wavefield and its inverse filter. There are very clear down-going and up-going arrivals in the full-wavefield section. These stack traces may be compared with surface seismic data.

For the zero-offset horizontal-vibration X-component data, only the common-receiver-depth stack section is plotted (Fig. 3). Inserted dummy traces are also shown. There were very few events after the first arrivals. The main result from this component data is the shear-wave arrival times as a function of depth.

Figure 4 shows sections for the other zero-offset source and receiver combinations: a) zero-offset vertical-vibration X-component data, b) zero-offset vertical-vibration Y-component data, c) zero-offset horizontal-vibration Y-component data and d) zero-offset horizontal-vibration Z-component data.

Velocity-depth plots

An important application of VSP data is to provide accurate velocity-depth data for the formation penetrated by the well. Downhole sonic logs provide substantially greater depth resolution, but the VSP results are much less subject to borehole conditions. They average over a much larger volume of the formation, so that they provide much more accurate absolute velocities. Figure 5 shows the compressional and shear-interval velocity versus depth based on the first-arrival picks of the X- and Z-component data. Figure 6 and Table 3 show the first-arrival picks.

The shear-wave interval velocities from the X-component data have much greater uncertainties than the compressional-wave velocities. Abnormally high shear-wave velocities from 950 to 1000 m may be due to the large uncertainties in first-arrival picks in this depth range. To examine the vertical resolution of the VSP velocity data, the calculated interval velocities were successively averaged over depth intervals ranging from 5 to 35 m. Figure 5 shows a comparison of 35 m and 15 m average P-wave interval velocities. Based upon the estimated accuracy of first-arrival picking, intervals of about 35 m appear to be the minimum for reliable velocities, but some of the rapid vertical changes of 200–500 m/s in the 15 m data may represent real velocity variations. Uncertainties of ~1 sample give ~3% or ~70 m/s velocity uncertainty for 35 m intervals. This is similar to the amplitudes of the high-frequency variability in the velocity-depth data, indicating that this is about the smallest spatial interval that can be resolved with the data.

The compressional velocities calculated from the first arrivals of offset vertical-vibration Z-component (Fig. 5) data have excellent agreement with those from the zero-offset data.

The compressional velocity-depth profile shows high velocities of 3000–3500 m/s decreasing downward to a depth of about 550 m. The velocities then decrease rapidly downward to about 2000 m/s at the base of permafrost near 600 m depth. From 640 to about 920 m, the velocities increase slowly as expected for simple loading sediment compaction,

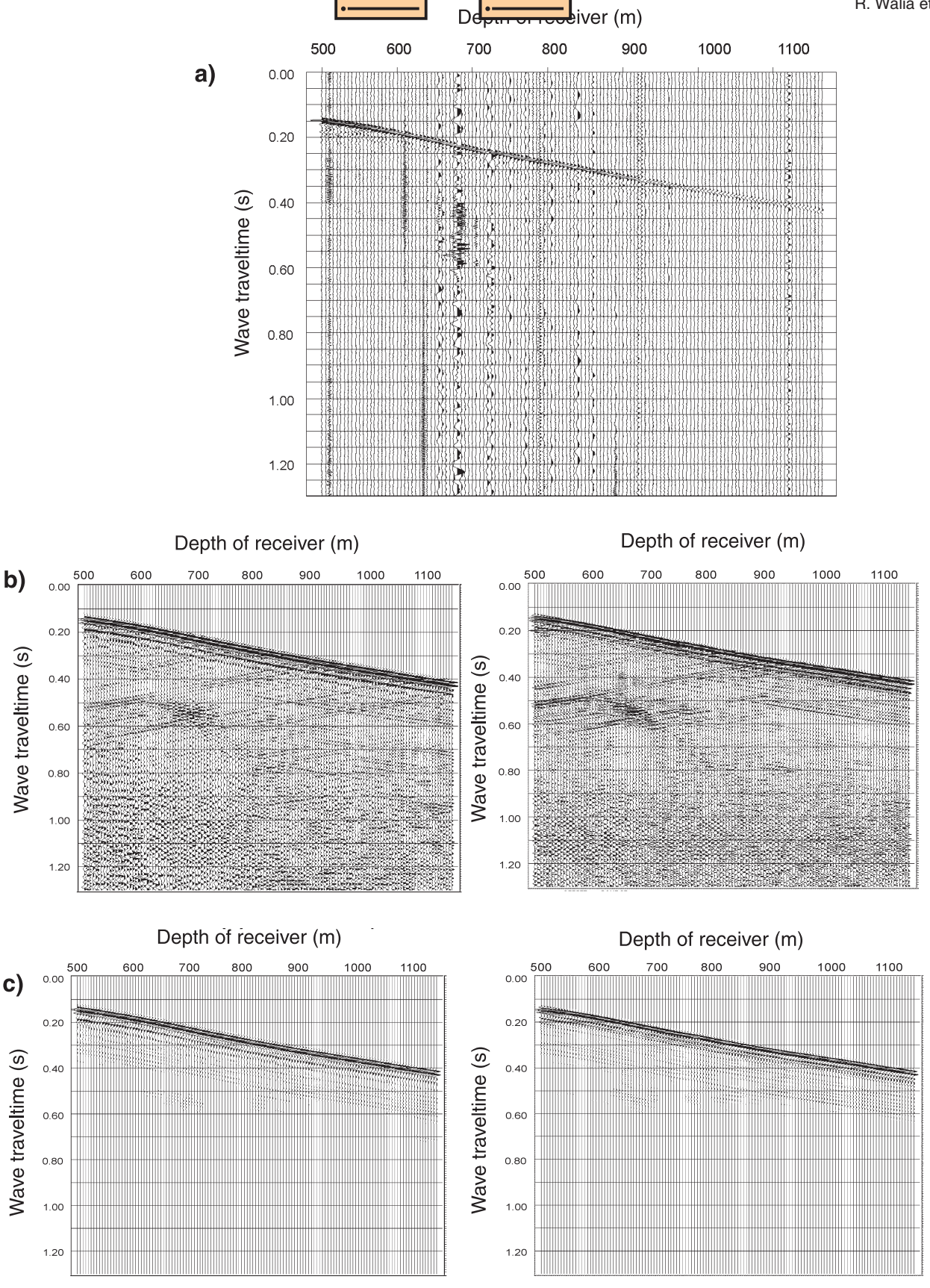

Figure 2. *Progressive steps in processing of the offset VSP Z-component data.* ***a)*** *Raw data of zero-offset vertical-vibration Z-component data.* ***b)*** *Common-depth stack section after F-X noise reduction.* ***c)*** *Down-going wavefield, no AGC (automatic gain control) applied.* ***d)*** *Up-going wavefield.* ***e)*** *Up-going wavefield aligned with first arrival.* ***f)*** *Corridor stack, Reiber mixing was not applied.* ***g)*** *Up-going wavefield after Reiber mixing.* ***h)*** *Wavelet estimated from down-going wavefield and its inverse filter.*

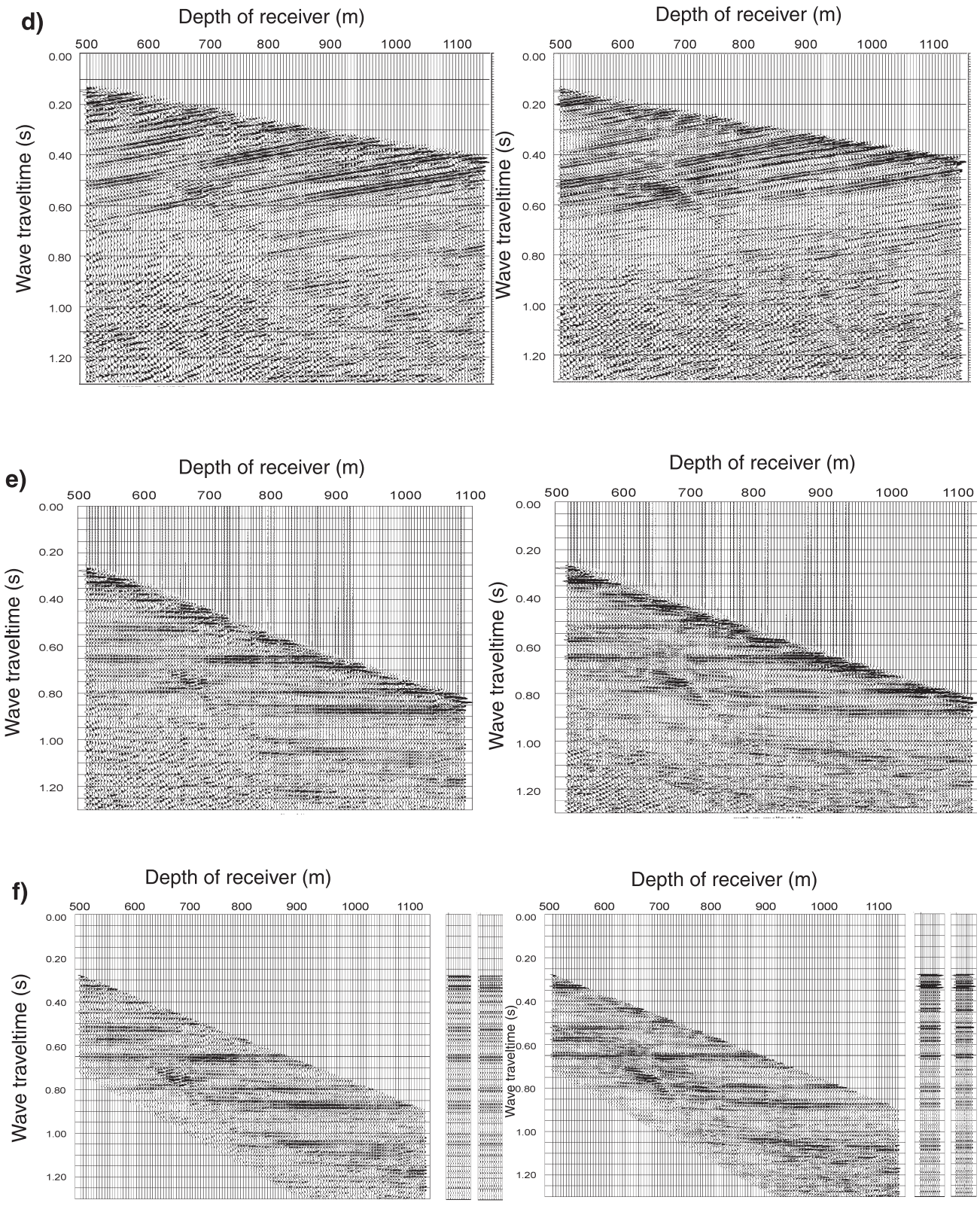

Figure 2. *(cont.)*

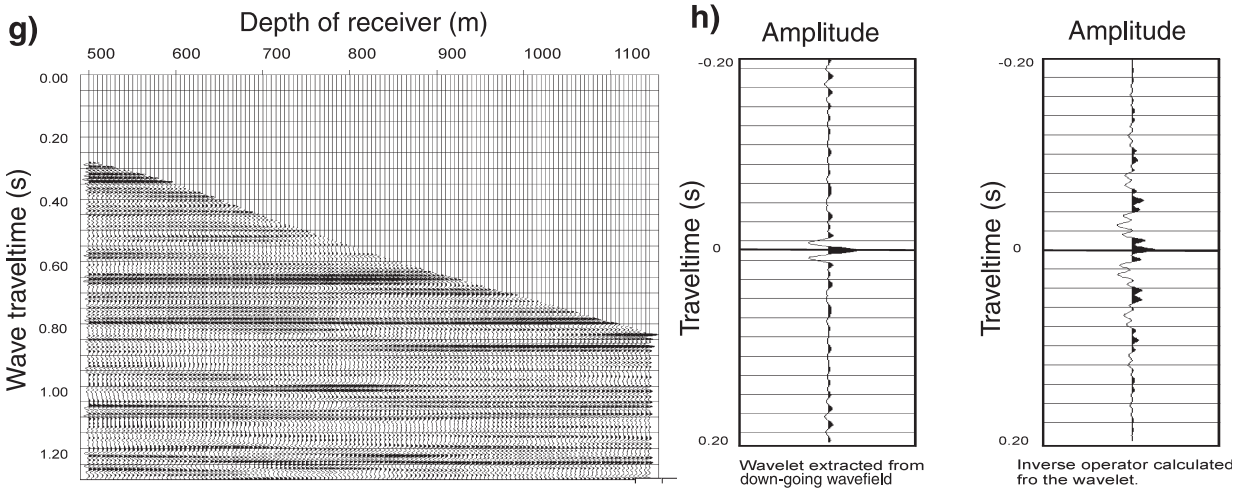

Figure 2. *(cont.)*

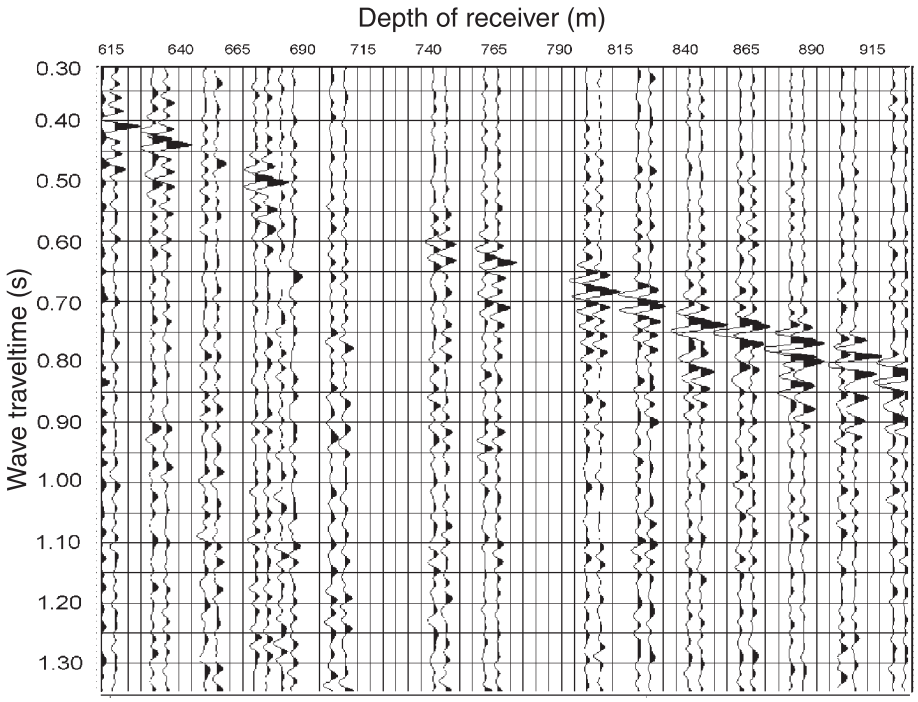

Figure 3. *Zero-offset horizontal-vibration X-component data. Dummy traces were inserted to form a regular depth interval.*

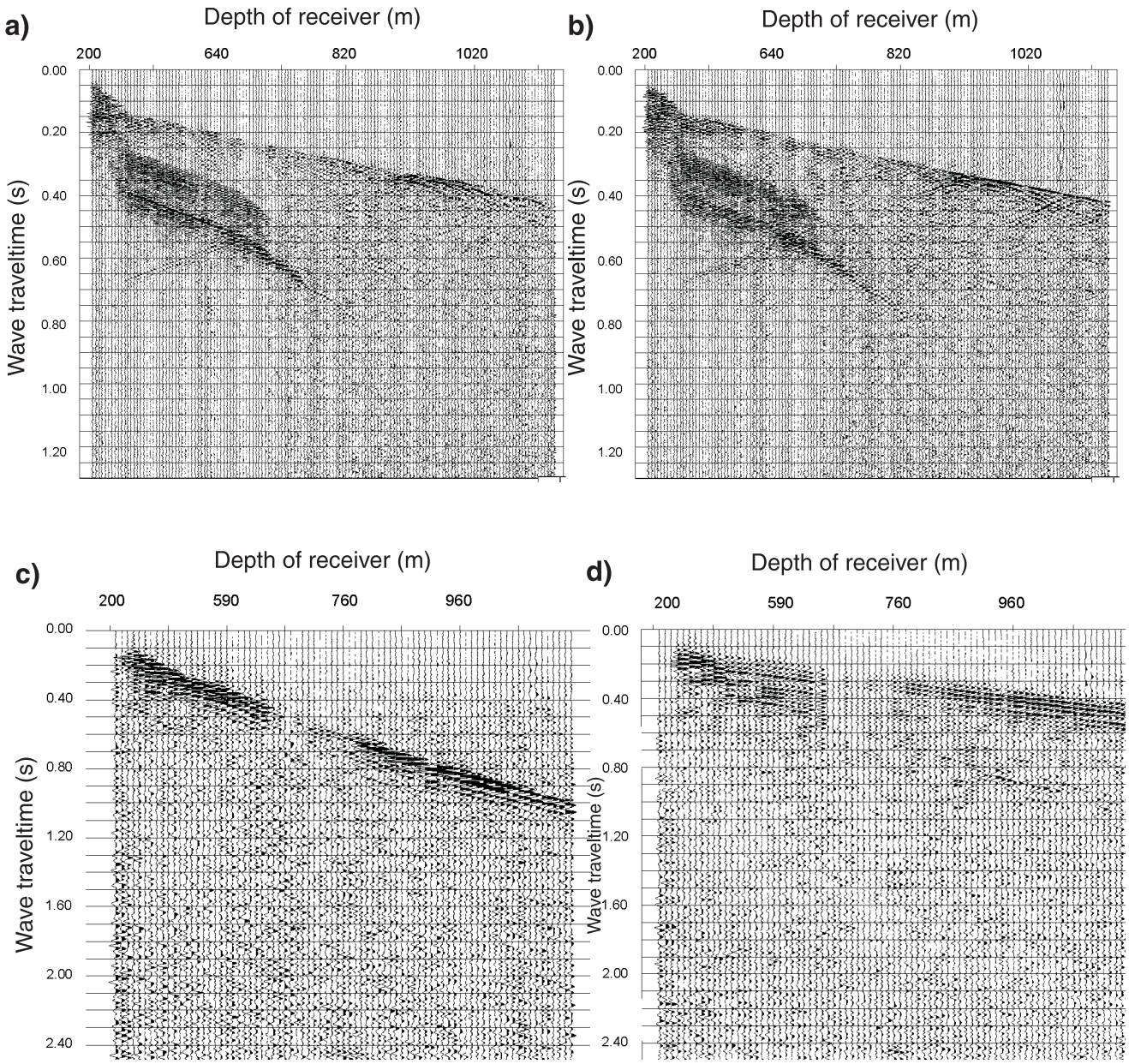

Figure 4. *Common-receiver-depth stack sections of the other components.* ***a)*** *Zero-offset vertical-vibration X-component.* ***b)*** *Zero-offset vertical-vibration Y-component.* ***c)*** *Zero-offset horizontal-vibration Y-component data.* ***d)*** *Zero-offset horizontal-vibration Z-component data.*

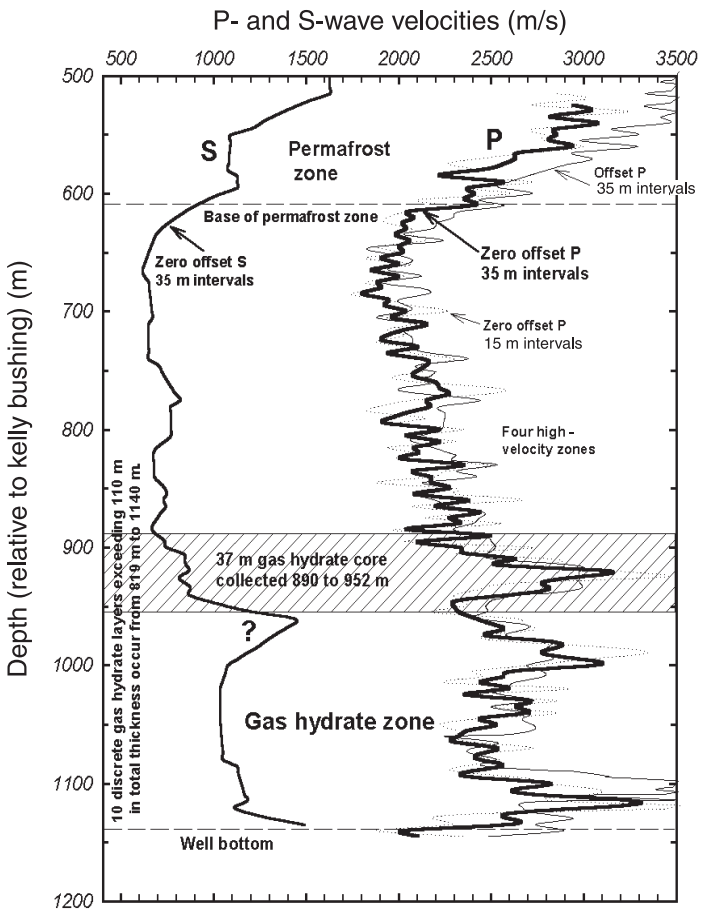

Figure 5.

Compressional- and shear-wave velocities calculated from first arrivals.

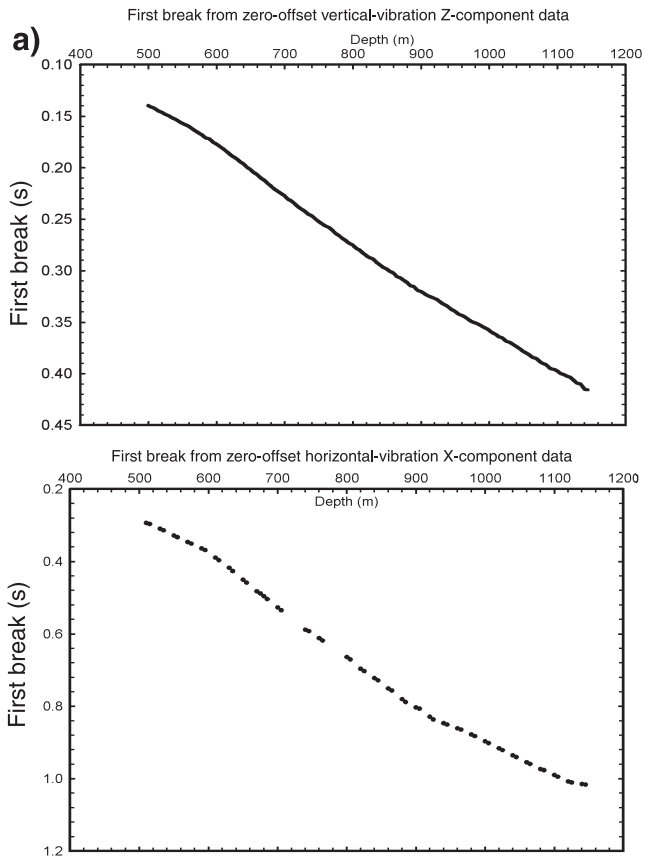

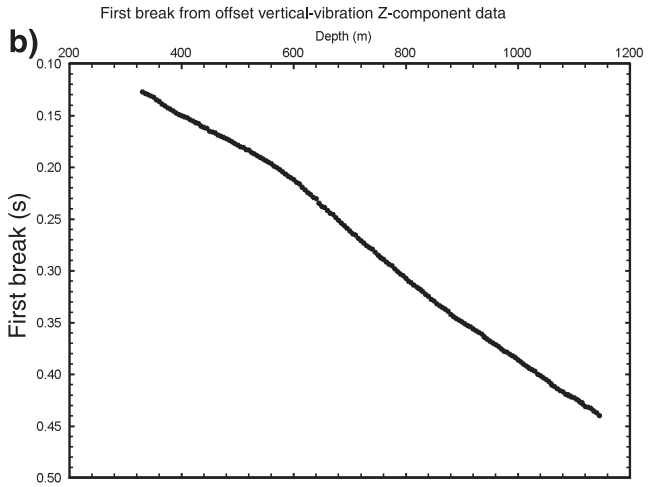

Figure 6.

a) *Time versus depth VSP data, (top) zero-offset P-wave; (bottom) zero-offset S-wave.* ***b)*** *Time versus depth VSP data from offset vertical-vibration P wave.*

Table 3a. First-arrival pairs picked from zero-offset vertical-vibration Z-component data.

Depth (m)	First arrival (s)	Depth (m)	First arrival (s)	Depth (m)	First arrival (s)	Depth (m)	First arrival (s)	Depth (m)	First arrival (s)
500	0.13963	630	0.1915	760	0.2565	890	0.31563	1020	0.36538
505	0.14125	635	0.19425	765	0.258	895	0.31888	1025	0.36825
510	0.14263	640	0.19638	770	0.2605	900	0.32013	1030	0.3695
515	0.14488	645	0.1995	775	0.26375	905	0.32213	1035	0.37138
520	0.14625	650	0.20175	780	0.26588	910	0.32413	1040	0.3735
525	0.14813	655	0.20463	785	0.26863	915	0.3255	1045	0.37563
530	0.1495	660	0.20675	790	0.27075	920	0.32688	1050	0.37813
535	0.1515	665	0.20988	795	0.27338	925	0.3285	1055	0.38
540	0.153	670	0.212	800	0.275	930	0.33113	1060	0.38213
545	0.155	675	0.215	805	0.27813	935	0.333	1065	0.38438
550	0.15688	680	0.21775	810	0.27988	940	0.335	1070	0.3855
555	0.15838	685	0.22063	815	0.28275	945	0.33763	1075	0.38838
560	0.16	690	0.22275	820	0.28525	950	0.33938	1080	0.39025
565	0.16238	695	0.225	825	0.28738	955	0.34188	1085	0.39188
570	0.1645	700	0.22725	830	0.28875	960	0.34338	1090	0.39488
575	0.16663	705	0.2305	835	0.29188	965	0.345	1095	0.39588
580	0.16863	710	0.23225	840	0.29425	970	0.34738	1100	0.39725
585	0.17125	715	0.235	845	0.29675	975	0.3495	1105	0.39975
590	0.17213	720	0.23788	850	0.29838	980	0.35075	1110	0.40088
595	0.175	725	0.24025	855	0.30075	985	0.35213	1115	0.4025
600	0.177	730	0.24238	860	0.30238	990	0.354	1120	0.40388
605	0.17925	735	0.24513	865	0.30563	995	0.35575	1125	0.40675
610	0.18163	740	0.24675	870	0.307	1000	0.35763	1130	0.40938
615	0.18425	745	0.2495	875	0.30938	1005	0.36025	1135	0.4105
620	0.187	750	0.25213	880	0.3115	1010	0.36188	1140	0.41475
625	0.18938	755	0.25438	885	0.31463	1015	0.36425	1145	0.41575

Table 3b. First-arrival pairs picked from zero-offset horizontal-vibration X-component data.

Depth (m)	First arrival (s)	Depth (m)	First arrival (s)	Depth (m)	First arrival (s)	Depth (m)	First arrival (s)	Depth (m)	First arrival (s)
510	0.29292	635	0.426	800	0.6635	925	0.836	1060	0.95425
515	0.296	650	0.45	805	0.67	940	0.8465	1065	0.959
530	0.30909	655	0.458	820	0.696	945	0.85	1080	0.97325
535	0.31345	670	0.482	825	0.7024	960	0.8605	1085	0.976
550	0.328	675	0.488	840	0.7216	965	0.864	1100	0.9895
555	0.33244	680	0.49571	845	0.728	980	0.8775	1105	0.994
570	0.34578	685	0.50343	860	0.7505	985	0.882	1120	1.0075
575	0.35022	700	0.52657	865	0.756	1000	0.8965	1125	1.01
590	0.36356	705	0.53429	880	0.78	1005	0.90133	1140	1.0145
595	0.368	740	0.58829	885	0.788	1020	0.91583	1145	1.016
610	0.389	745	0.592	900	0.803	1025	0.92067		
615	0.396	760	0.6115	905	0.806	1040	0.93517		
630	0.417	765	0.618	920	0.8285	1045	0.94		

Table 3c. First-arrival pairs picked from offset horizontal-vibration Z-component data.

Depth (m)	First arrival (s)	Depth (m)	First arrival (s)	Depth (m)	First arrival (s)	Depth (m)	First arrival (s)	Depth (m)	First arrival (s)
330	0.12713	510	0.18063	690	0.25625	850	0.329	1019	0.3935
335	0.12863	515	0.18288	695	0.25875	855	0.33175	1020	0.394
340	0.12963	520	0.18325	700	0.26138	860	0.33363	1025	0.39538
345	0.131	525	0.18575	705	0.26413	865	0.33525	1030	0.39688
350	0.13213	530	0.187	710	0.26525	870	0.33688	1035	0.39988
355	0.13475	535	0.18863	715	0.2685	875	0.33888	1040	0.40125
360	0.13625	540	0.19025	720	0.27088	880	0.34213	1045	0.40313
365	0.13888	545	0.19175	725	0.27313	885	0.34425	1050	0.40488
370	0.1405	550	0.1935	730	0.27563	890	0.346	1055	0.40688
375	0.1425	555	0.195	735	0.2775	895	0.34763	1059	0.40888
380	0.14375	560	0.19638	740	0.27888	900	0.34913	1060	0.41025
385	0.1455	565	0.19888	745	0.28188	905	0.351	1065	0.41175
390	0.14738	570	0.20013	750	0.28463	910	0.35275	1070	0.41375
395	0.14888	575	0.20225	751	0.285	915	0.354	1075	0.41563
400	0.15013	580	0.20425	755	0.287	920	0.356	1080	0.41675
405	0.15113	585	0.2065	756	0.28775	925	0.35775	1085	0.41913
410	0.152	590	0.2085	760	0.28888	930	0.35938	1089	0.4195
415	0.15388	595	0.21013	765	0.29138	935	0.36088	1090	0.42038
420	0.15513	600	0.21175	770	0.2935	939	0.36313	1094	0.421
425	0.15675	605	0.2145	775	0.29488	940	0.364	1095	0.42163
430	0.15763	610	0.21588	780	0.298	944	0.3655	1100	0.4225
435	0.16025	615	0.21925	785	0.30038	945	0.366	1105	0.42413
440	0.16138	620	0.22175	790	0.30288	950	0.36788	1109	0.42575
445	0.16225	625	0.22438	795	0.3045	955	0.3695	1110	0.42663
450	0.16513	630	0.22625	800	0.30713	960	0.37125	1114	0.42725
455	0.16575	635	0.229	805	0.31	965	0.37288	1115	0.4285
460	0.16675	640	0.23013	809	0.31138	970	0.37525	1120	0.431
465	0.16888	645	0.23463	814	0.31375	975	0.3775	1125	0.43163
470	0.16988	650	0.23763	820	0.31575	980	0.3785	1130	0.43263
475	0.17113	655	0.23875	822	0.31675	985	0.38038	1135	0.43525
480	0.17238	660	0.24163	825	0.31763	990	0.382	1140	0.437
485	0.17375	665	0.24425	827	0.31863	995	0.38363	1145	0.43975
490	0.17525	670	0.2455	830	0.31988	1000	0.38588		
495	0.177	675	0.2485	835	0.32263	1005	0.38788		
500	0.17838	680	0.25125	840	0.3245	1010	0.39013		
505	0.18013	685	0.25388	845	0.3275	1015	0.39188		

until higher and irregular velocities are reached in the gas hydrate layer below about 900 m. Higher velocity layers are observed at about 925 m, 975 m, and 1100 m. The general high-velocity zone below about 900 m, averaging 2600 m/s, corresponds to the zone of gas hydrate layers cored or inferred from other data. The especially high velocity layer centred at about 925 m corresponds to the 37 m gas hydrate core collected between 890 and 952 m. One especially high velocity peak is located at about 1100 m depth, just above the base of the hole. There are lower velocities at the very bottom of the hole near the base of hydrate stability, but they are not well resolved. Comparison with the downhole sonic-log velocity profile shows good correspondence, both in absolute velocities and in the location of high-velocity layers that are interpreted to represent high gas hydrate concentrations (Sakai, 1998, 1999).

Shear wave and Poisson's Ratio

The zero-offset shear-wave velocities (Fig. 5) have lower resolution than the compressional velocities, but give important constraints on the effect of gas hydrate on elastic parameters. The different dependence of P- and S-wave velocities on hydrate concentration provides constraint on the location of the gas hydrate, i.e. whether it is located mainly at grain boundary contacts and increases frame stiffness, or is mainly in pore spaces and does not affect cementing grain contacts. The effect of gas hydrate on Poisson's Ratio is also important for amplitude-versus-offset (AVO) and full-waveform modelling (e.g. Yuan et al., 1999). In the unfrozen section between about 640 and 920 m, Poisson's Ratio is a nearly constant 0.44, nearly independent of the downward increase in velocity. In both the permafrost section above about 600 m,

and the gas hydrate section below about 920 m, Poisson's Ratio is about 0.39 (Fig. 7). Thus the effect on elastic moduli of the gas hydrate is similar to that of the permafrost ice.

The Poisson's Ratio (Fig. 7) average of 0.44 in the unfrozen section is in good agreement with the general relation of Castagna et al. (1985) for clastic sediments ('mud rocks'). The Castagna et al. relation predicts Poisson's Ratios of 0.43–0.45 for the compressional velocities of 2000–2300 m/s measured in this section (Fig. 8). The Poisson's Ratio is much lower, about 0.39 in both the permafrost zone and the zone of gas hydrate. The Poisson's Ratio agreement between the latter two sections indicates that ice and gas hydrate have a similar affect on the sediment elastic modulii. The Poisson's Ratio of 0.39 in the frozen sections is also in agreement with that of about 0.39, predicted by the Castagna et al. relation for the observed velocities of about 2600 m/s. Thus, the effect of both gas hydrate and ice on the Poisson's Ratio is similar to that from reduction in porosity by simple compaction.

Both the frozen and unfrozen sections agree well with the relation for clastic rocks between Vp and Poisson's Ratio given by Castagna et al. (1985) for simple compaction. This suggests that the effect of the ice and gas hydrate is approximately the same as that for simple addition to the sediment-grain matrix and porosity reduction. This was the approximation used by Hyndman and Spence (1992) for estimating marine gas hydrate concentrations from velocity increase relative to a no-hydrate reference velocity. The time-average relation gives a similar result (summary by Yuan et al., 1996). Small amounts of gas hydrate would impose a much larger effect on velocity if the gas hydrate cemented grain

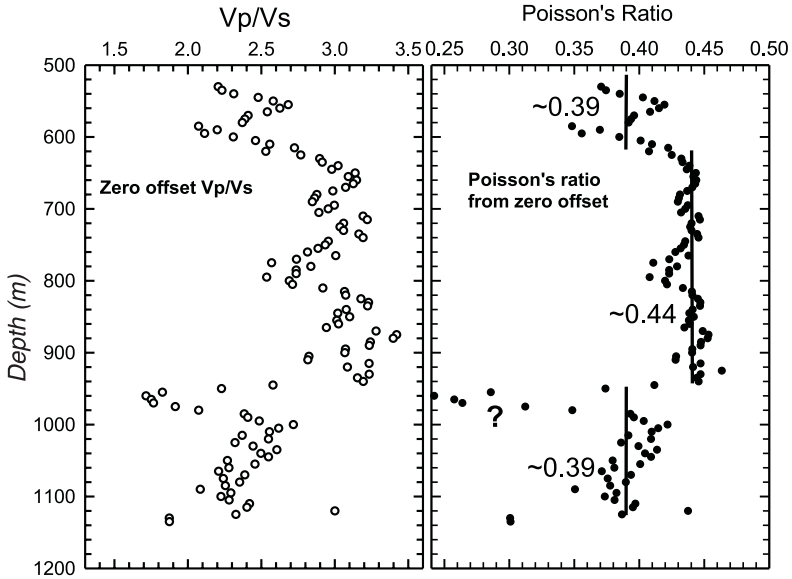

Figure 7.

Vp/Vs and Poisson's Ratio as a function of depth from zero-offset data.

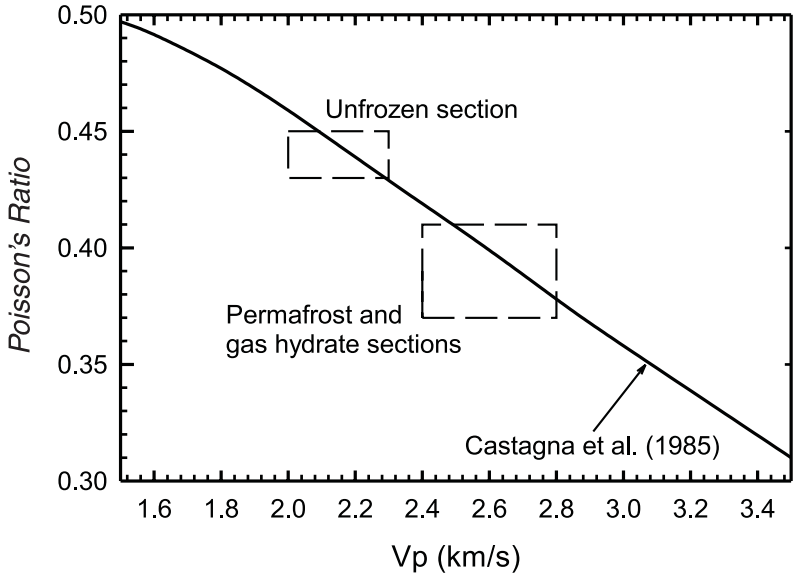

Figure 8.

Poisson's Ratio as a function of Vp from Castagna et al. (1985).

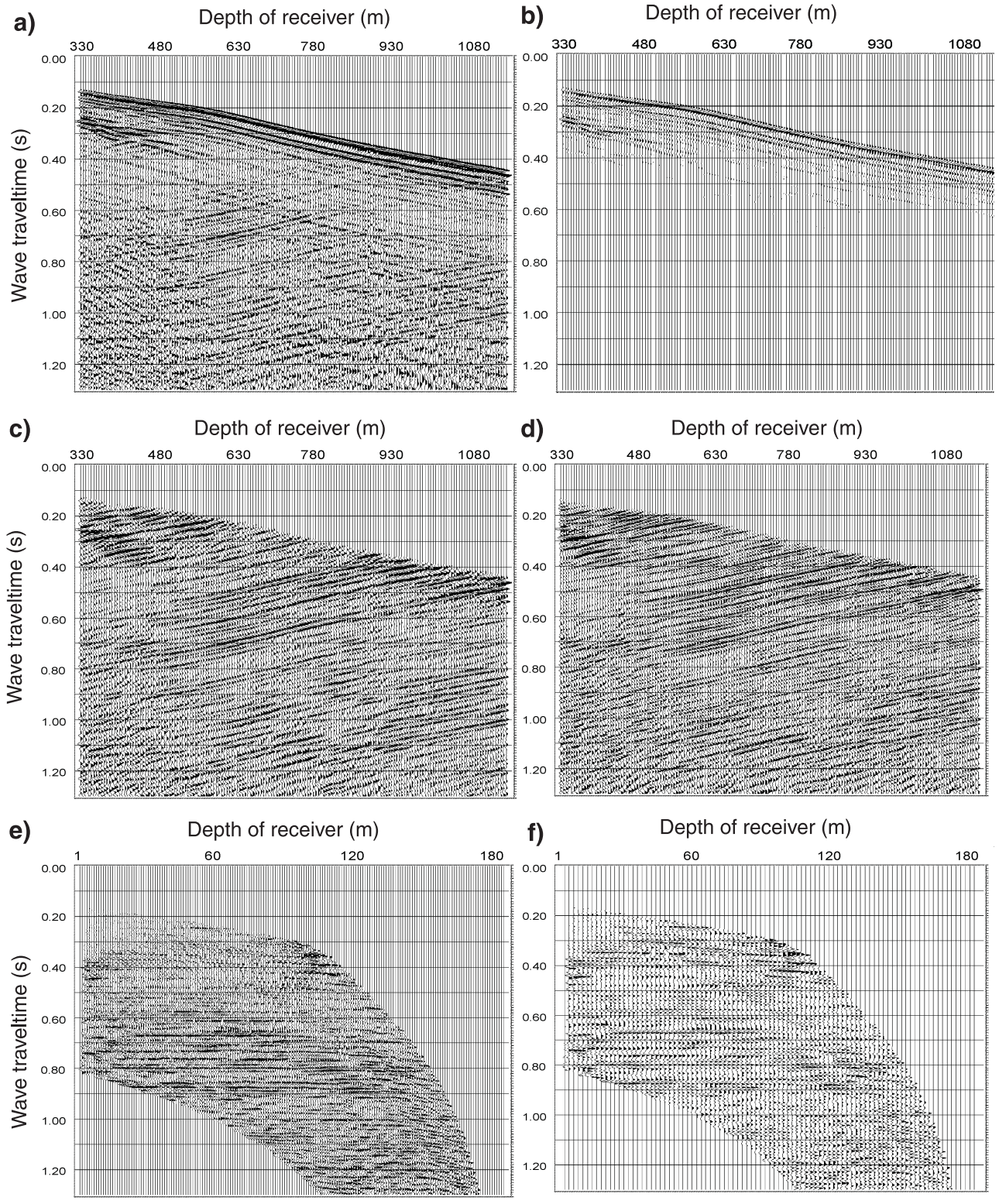

Figure 9. *Wavelet-processing steps of the offset Z-component data.* ***a)*** *Common-receiver-depth stack.* ***b)*** *Down-going wavefield.* ***c)*** *Up-going wavefield before inverse filter.* ***d)*** *Up-going wavefield after inverse filter.* ***e)*** *VSP-CDP transformation, 1 m CDP interval.* ***f)*** *VSP-CDP transformation, 2 m CDP interval.*

boundaries, rather than being located in the pore spaces. Sakai (1999) gave a further analysis of the implications for the effect of gas hydrate on elastic modulii and different theoretical models.

Offset data

Both wavelet-processing and zero-phase spiking-deconvolution methods have been applied to offset vertical-vibration Z-component data. Figure 9 shows the progressive processing steps in the wavelet-processing flow. VSP-CDP transformation using 1 m and 2 m CDP (common depth point) interval are also shown. Such VSP-CDP transformation sections can be directly compared with the surface seismic data. The X and Y components have been stacked (Fig. 10). However, we have not yet been able to successfully separate the P and S wavefields, especially the up-going P and S wavefields.

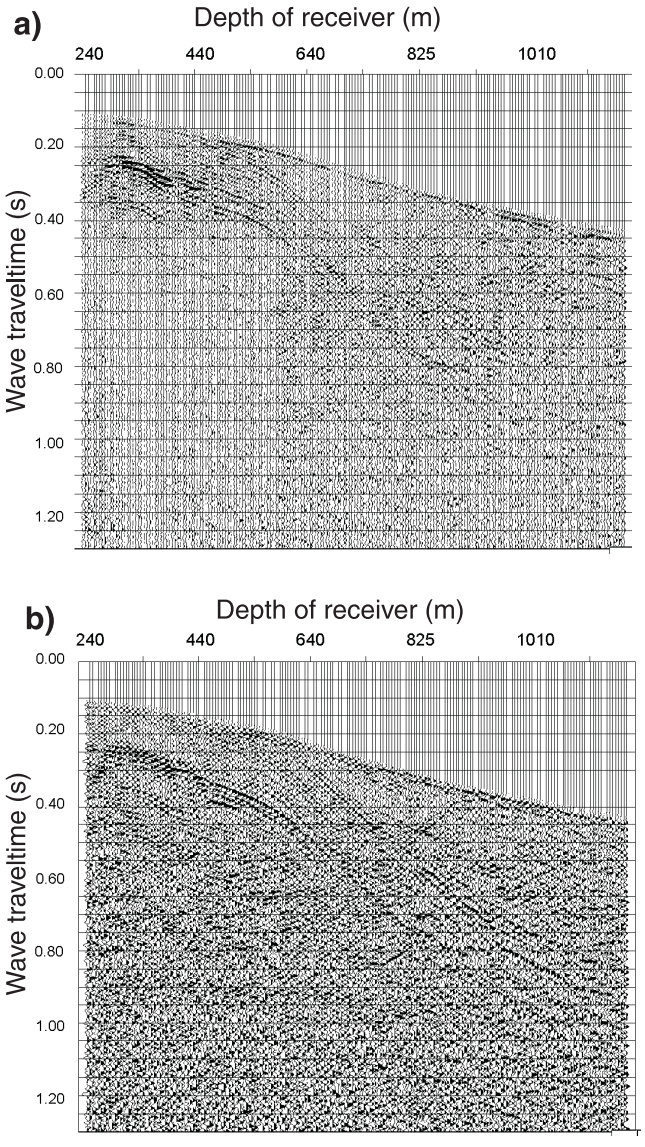

Figure 10. *Common-depth-receiver stack of offset X- and Y-component data.* ***a)*** *Offset source, X-component stack.* ***b)*** *Offset source, Y-component stack.*

CONCLUSIONS

Initial analyses of the VSP data from the Mallik gas hydrate well show high-quality signals with good signal-to-noise ratios. There are numerous strong arrivals in the up-going and down-going wavefields for the compressional data that were readily separated in the processing. The corridor stack provides a good comparison with surface seismic-reflection data, allowing accurate depth determination and, using the well data, reliable identification of reflectors in the surface-reflection data. The compressional-wave velocity-depth profile from the VSP appears to be very accurately determined, with a vertical resolution of at least 35 m. Initial analysis of the offset compressional-wave data gives a velocity-depth profile that is in excellent agreement with that from the zero-offset data. The shear-wave velocity-depth profile is less well determined, but it is sufficiently accurate to give very useful estimates of Poisson's Ratio with depth. A zone of uncertain shear velocities is also noted.

Poisson's Ratio (Fig. 7) averages about 0.44 in the unfrozen section, which is in good agreement with the general relation of Castagna et al. (1985) for clastic sediments. The Castagna et al. relation predicts Poisson's Ratios of 0.43–0.45 for the compressional velocities of 2000–2300 m/s measured in this section. The Poisson's Ratio is much lower, about 0.39, in both the permafrost zone and the zone of gas hydrate. The Poisson's Ratio agreement between the permafrost and gas hydrate sections suggests that ice and gas hydrate have a similar affect on the sediment elastic moduli. The Poisson's Ratio of 0.39 in the frozen sections is also in agreement with that of about 0.39 predicted by the Castagna et al. (1985) relation for the observed velocities of about 2600 m/s. Thus, the effect of both gas hydrate and ice on the Poisson's Ratio is similar to that from reduction in porosity by simple compaction. The frozen material must be primarily in the sediment pores, rather than concentrated at the grain boundary contacts.

ACKNOWLEDGMENTS

We acknowledge the excellent field operations by Schlumberger Ltd. for the VSP survey, and overall science program management for the project by S.R. Dallimore, T. Uchida, and T.S. Collett.

REFERENCES

Castagna, J.P., Batzle, M.L., and Eastwood, R.L.
1985: Relationships between compressional-wave and shear-wave velocities in clastic silicate rocks, Geophysics, v. 50, p. 571–581.

Dallimore, S.R., Collett, T.S., and Uchida, T.
1999: Overview of science program, JAPEX/JNOC/GSC Mallik 2L-38 gas hydrate research well; *in* Scientific Results from JAPEX/JNOC/GSC Mallik 2L-38 Gas Hydrate Research Well, Mackenzie Delta, Northwest Territories, Canada, (ed.) S.R. Dallimore, T. Uchida, and T.S. Collett; Geological Survey of Canada, Bulletin 544.

Hardage, B.A.
1983: Vertical seismic profiling, part A: principles; Geophysical Press, London-Amsterdam.

Hyndman, R.D. and Spence, G.D.
1992: A seismic study of methane hydrate seafloor bottom-simulating reflectors, Journal of Geophysical Research, v. 97, p. 6683–6698.

Sakai, A.
1998: Vertical seismic survey in the Mallik 2L-38 — specifications, data acquisitions and data analysis; *in* Proceedings of the International Symposium on Methane Hydrates: Resources in the Near Future?, Japan National Oil Corporation–Technical Research Center, Chiba City, Japan, p.359–370.

1999: Velocity analysis of vertical seismic profile (VSP) survey at Mallik 2L-38 gas hydrate research well, and related problems for estimating gas hydrate concentration; *in* Scientific Results from JAPEX/JNOC/GSC Mallik 2L-38 Gas Hydrate Research Well, Mackenzie Delta, Northwest Territories, Canada, (ed.) S.R. Dallimore, T. Uchida, and T.S. Collett; Geological Survey of Canada, Bulletin 544.

Toksoz M.N. and Stewart, R.R.
1983: Vertical seismic profiling, part B: advanced concepts, Geophysical Press, London-Amsterdam.

Yuan, T., Hyndman, R.D., Spence, G.D., and Desmons, B.
1996: Seismic velocity increase and deep-sea gas hydrate concentration above a bottom-simulating reflector on the northern Cascadia continental slope, Journal of Geophysical Research, v. 101, p. 13 655–13 671.

Yuan, T., Spence, G.D., Hyndman, R.D., Minshull, T.A., and Singh, S.C.
1999: Seismic velocity studies of a gas hydrate bottom-simulating reflector on the northern Cascadia continental margin: amplitude modeling and full waveform inversion; Journal of Geophysical Research, v. 104, p. 1179–1191.